THE JOURNAL OF PHYSICAL CHEMISTRY A

Article

pubs.acs.org/JPCA

Kinetics of the NCN + NO Reaction over a Broad Temperature and Pressure Range

Oliver Welz† and Matthias Olzmann*

Institut für Physikalische Chemie, Karlsruher Institut für Technologie (KIT), Kaiserstrasse 12, 76131 Karlsruhe, Germany

Supporting Information

ABSTRACT: Rate coefficients for the reaction ^{3}NCN + NO → products (R3) were measured in the temperature range 251−487 K at pressures from 10 mbar up to 50 bar with helium as the bath gas. The experiments were carried out in slow-flow reactors by using pulsed excimer laser photolysis of NCN_3 at 193 or 248 nm for the production of NCN. Pseudo-first-order conditions ($[NCN]_0 \ll NO$) were applied, and NCN was detected time-resolved by resonant laser-induced fluorescence excited near 329 nm. The measurements at the highest pressures yielded values of $k_3 \sim 8 \times 10^{-12}$ cm^3 s^{-1} virtually independent of temperature and pressure, which indicates a substantially smaller high-pressure limiting value of k_3 than predicted in earlier works. Our experiments at pressures below 1 bar confirm the negative temperature and positive pressure dependence of the rate coefficient k_3 found in previous investigations. The falloff behavior of k_3 was rationalized by a master equation analysis based on a barrierless association step ^{3}NCN + NO ↔ NCNNO(^{2}A″) followed by a fast internal conversion NCNNO(^{2}A″) ↔ NCNNO(^{2}A′). From 251−487 K and above 30 mbar, the rate coefficient k_3 is well represented by a Troe parametrization for a recombination/dissociation reaction, $k_3(T,P) = k_4^{\infty}k_4^{0}[M]F(k_4^{0}[M] + k_4^{\infty})^{-1}$, where k_4 represents the rate coefficient for the recombination reaction ^{3}NCN + NO. The following parameters were determined (30% estimated error of the absolute value of k_3): k_4^{0}[M=He] = $1.91 \times 10^{-30}(T/300\ K)^{-3.3}$ cm^6 s^{-1}[He], $k_4^{\infty} = 1.12 \times 10^{-11} \exp(-23\ K/T)$ cm^3 s^{-1}, and $F_C = 0.28 \exp(173\ K/T)$.

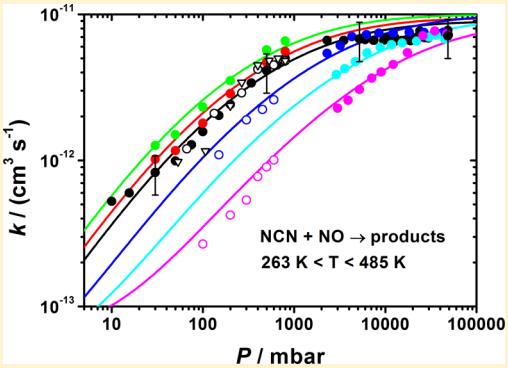

1. INTRODUCTION

Nitric oxide (NO) is a major pollutant emitted into the atmosphere from internal combustion engines and other combustion devices.[1,2] Besides causing adverse health effects, it contributes to formation of photochemical smog in the troposphere and ozone depletion in the stratosphere.[2] To minimize these emissions, a fundamental understanding of the reactions governing NO formation is required.

Several pathways can lead to NO in combustion processes. Their relative contributions depend on temperature, pressure, stoichiometry, and fuel structure.[1] Under fuel-rich conditions, so-called prompt NO formation can become important. This phenomenon was originally discovered by Fenimore,[3] who observed that the NO concentration in the postflame zone extrapolated to the flame front position was nonzero for hydrocarbon fuels. Fenimore suggested that reactions of small hydrocarbon radicals with N_2 might produce nitrogen-containing species, which are readily oxidized to form NO. As one initial step, the spin-forbidden reaction

$$^2CH + N_2 \rightarrow {}^4N + HCN \qquad (R1)$$

was proposed[3] and later incorporated in nitrogen combustion submechanisms (see, e.g., refs 4 and 5). However, subsequent theoretical studies conclusively showed[6] that the spin conversion from the doublet to the quartet state is too slow to be compatible with experimental findings on the kinetics of the CH + N_2 reaction. This apparent discrepancy was resolved by Moskaleva and Lin.[7] Their quantum chemical calculations suggested the spin-allowed channel

$$^2CH + N_2 \rightarrow {}^3NCN + {}^2H \qquad (R2)$$

as an alternative to R1. The existence of this channel was experimentally confirmed by Vasudevan et al.,[8] who detected NCN as a direct product from the reaction of ^{2}CH with N_2 in a shock tube. In a recent theoretical study, Harding et al.[9] could quantitatively reproduce the experimental kinetic results for the ^{2}CH + N_2 reaction on the basis of eq R2, employing multireference ab initio and master equation calculations. The first direct detection of NCN in a flame was reported by Smith,[10] and it could be shown[10,11] that in low-pressure methane−air flames the concentrations of NCN and CH are correlated. These results clearly indicate that reaction R2 has to be incorporated in the mechanism for prompt NO formation.[12−16] Accordingly, reliable kinetic data on NCN reactions are needed.[17] The lack of such data stimulated several studies on NCN reactions over the past decade (see, e.g., the literature cited in ref 18).

Received: March 30, 2012
Revised: May 14, 2012
Published: June 13, 2012

   dx.doi.org/10.1021/jp303069g | J. Phys. Chem. A 2012, 116, 7293−7301

In the present work, we report on a kinetic study of the reaction

$$NCN + NO \rightarrow \text{products} \quad (R3)$$

This reaction was first investigated by Baren and Hershberger,[19] who determined rate coefficients in the temperature range 298−573 K at pressures of 4, 400, and 800 mbar with helium as the bath gas. Laser flash photolysis of diazomethane (CH_2N_2) in the presence of cyanogen (C_2N_2) was used for production of NCN, which was detected time-resolved by laser-induced fluorescence (LIF) near 329 nm.[20] A positive pressure and negative temperature dependence of k_3 was observed and attributed to NCNNO adduct formation. The authors assumed the value of $k_3 = (5.0 \pm 0.5) \times 10^{-12}$ cm^3 s^{-1} obtained at T = 298 K and P = 800 mbar as a high-pressure limit.

Huang et al.[21] determined rate coefficients of reaction R3 in the temperature range 254−353 K at pressures between 40 and 800 mbar with both He and N_2 as bath gas. Laser photolysis of cyanogen azide (NCN_3) at 193 nm was used to produce NCN, and resonant LIF of NCN at 329.01 nm was employed to monitor the reaction. The temperature and pressure dependence of the rate coefficients k_3 obtained are essentially in line with the results from ref 19. The experiments were supplemented by quantum chemical calculations at the G2M(CC5)[22] level of theory. A schematic potential energy diagram is displayed in Figure 1. The calculations favor a

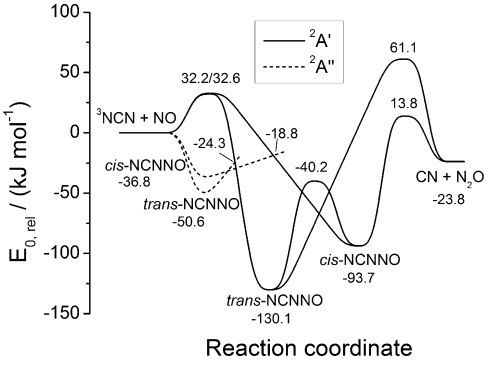

Figure 1. Potential energy diagram obtained at the G2M(CC5) level of theory adopted from ref 21. Only the kinetically most relevant pathways are displayed.

complex-forming mechanism via a chemically activated NCNNO intermediate:

$$NCN + NO + M \leftrightarrow NCNNO + M \quad (R4,-4)$$

$$NCNNO + M \rightarrow CN + N_2O + M \quad (R5)$$

The NCNNO intermediate has C_s symmetry and therefore can exist in both ^{2}A′ and ^{2}A″ electronic states. NCNNO (^{2}A′) is the electronic ground state and is more stable than the reactants by 130.1 (trans) and 93.7 (cis) kJ mol^{-1}, respectively. The excited ^{2}A″ state of NCNNO is stabilized by 50.6 kJ mol^{-1} (trans) and 36.8 kJ mol^{-1} (cis) relative to NCN + NO. Interestingly, formation of NCNNO from NCN + NO in the less stable electronic state ^{2}A″ was found to be barrierless, whereas for the more stable ^{2}A′ state barriers of 32.6 and 32.2 kJ mol^{-1} have to be surmounted for the cis and trans isomer, respectively. Crossing points between the ^{2}A″ and ^{2}A′ states of NCNNO were found, which are located 24.3 (trans) and 18.8 (cis) kJ mol^{-1} below the energy of NCN + NO, respectively. The product channel with the lowest barrier forms CN + N_2O, and this product pair is connected to the cis isomer in the ^{2}A′ state via a barrier of 37.6 kJ mol^{-1} (corresponding to 13.8 kJ mol^{-1} relative to NCN + NO).

Master equation calculations were performed in ref 21 on the basis of the following mechanism:

$$NCN + NO \leftrightarrow cis\text{-}NCNNO(^2A'') \quad (R6)$$

$$NCN + NO \leftrightarrow trans\text{-}NCNNO(^2A'') \quad (R7)$$

$$cis\text{-}NCNNO(^2A'') \leftrightarrow cis\text{-}NCNNO(^2A') \quad (R8)$$

$$trans\text{-}NCNNO(^2A'') \leftrightarrow trans\text{-}NCNNO(^2A') \quad (R9)$$

$$cis\text{-}NCNNO(^2A') \rightarrow CN + N_2O \quad (R10)$$

$$trans\text{-}NCNNO(^2A') \rightarrow CN + N_2O \quad (R11)$$

The NCN + NO association reactions, (R6) and (R7), were described with variational transition state theory, and a transition probability of unity was assumed for the crossings of the ^{2}A″ and ^{2}A′ states, (R8) and (R9). The tight exit channels (R10) and (R11) were modeled with RRKM theory. Within the experimental uncertainty, the master equation calculations reproduced the observed temperature and pressure dependence of k_3. Though not explicitly given, it is obvious from Figure 5 of ref 21 that a high-pressure limiting rate coefficient $k_3^\infty > 3 \times 10^{-11}$ cm^3 s^{-1} at 298 K would be predicted from the master equation calculations.

Two further theoretical studies[23,24] were published in 2005 about the mechanism of the NCN + NO reaction. Potential energy surfaces were calculated using the G2M(RCC,MP2)[23] and G2M(CC3)[24] methods, respectively. Although similar levels of theory were used, the potential energy surfaces differ substantially from each other and from the results of Huang et al.[21] In both refs 23 and 24 no distinction was made between the ^{2}A′ and ^{2}A″ states of NCNNO. Wei et al.[24] predicted a barrierless addition reaction R4 with stabilization energies of ∼208/182 kJ mol^{-1} for the *trans*/*cis*-NCNNO adduct, which significantly differ from the values of ∼130/94 kJ mol^{-1} for NCNNO (^{2}A′) reported by Huang et al.[21] In contrast, Chen and Ho[23] obtained barriers of ∼12 (cis) and ∼19 kJ mol^{-1} (trans) for the addition reaction R4, whereas the stabilization energies of the NCNNO conformers are in gross agreement with the values from Huang et al.[21]

The first high-temperature study of reaction R3 was published very recently by Dammeier and Friedrichs.[25] From their shock tube experiments, these authors obtained rate coefficients in the temperature range 764−1944 K at pressures between 123 and 690 mbar (argon), which can be represented by the Arrhenius equation $k_3 = 3.2 \times 10^{-12} \exp(-26.3 \text{ kJ mol}^{-1}/RT)$ cm^3 s^{-1}. At 764 K this expression corresponds to a rate coefficient of $k_3 = 5.0 \times 10^{-14}$ cm^3 s^{-1}, which is smaller than the values obtained at lower temperatures in refs 19 and 21. Taking additionally into account the switch from a negative (low T) to a positive (high T) temperature dependence of the rate coefficient, a change in the reaction mechanism from dominating addition at lower temperatures to preferential abstraction at higher temperatures[25] seems likely in general agreement with the predictions from ref 21.

The reverse reaction

$$CN + N_2O \rightarrow \text{products} \quad (R12)$$

dx.doi.org/10.1021/jp303069g | J. Phys. Chem. A 2012, 116, 7293−7301

was experimentally studied by Wang et al.[26] between 300 and 740 K in the pressure range 113−420 mbar with argon as the bath gas. A pressure-independent rate coefficient k_{12} was observed with a temperature dependence corresponding to an activation energy of 29.6 kJ mol^{-1}. From BAC-MP4 calculations, the authors concluded that the dominant product channel is NCN + NO. The observed activation energy is in reasonable agreement to the barrier height of 37.6 kJ mol^{-1} predicted for the reverse reaction of R10 by Huang et al.[21] (cf. Figure 1), who were able to reproduce the absolute value and temperature dependence of k_{12} in their calculations.

The aim of the present work was to study reaction R3 over an extended pressure range, in particular at pressures distinctly above 1 bar to determine rate coefficients at or close to the high-pressure limit. To the best of our knowledge, no experimental kinetic data in this pressure range are available yet. Our results can serve as a validation of the model predictions for k_3^∞ from ref 21 and the estimation from ref 19. We also performed experiments at pressures below 1 bar to test our experimental approach and to extend the existing data set in this range. The rate coefficients $k_3(T,P)$ obtained under these conditions can be directly compared with values from the literature.[19,21] On the basis of this combined experimental data set, which covers a pressure range from 10 mbar to 50 bar and a temperature range from 251 to 487 K, we performed a master equation analysis to rationalize the reaction mechanism and to parametrize the temperature and pressure dependence of k_3 for modeling purposes.

2. EXPERIMENTAL SECTION

2.1. General Approach. The experiments were performed employing the pulsed laser photolysis/laser-induced fluorescence technique in two different quasi-static reactors (see below) with helium as the bath gas. The NCN species was produced from NCN_3[27−30] at 193 or 248 nm with an ArF or KrF excimer laser, respectively. Upper limits (see below) of the NCN_3 concentration ranged from 2×10^{12} to 1×10^{14} cm^{-3} in the low-pressure experiments, and 3×10^{14} to 2×10^{16} cm^{-3} in the high-pressure experiments. To ensure pseudo-first-order conditions ($[NCN]_0 \ll [NO]$), we used NO in excess over NCN_3, typically on the order of 100−1000 in the low-pressure experiments and on the order of 10 in the high-pressure experiments. Resonant LIF was used for the time-resolved detection of NCN after excitation of the A $^3\Pi_u \leftarrow$ X $^3\Sigma_g^-$ transition near 329 nm[31] with a frequency-doubled dye laser (dye: DCM, 4-(dicyanomethylene)-2-methyl-6-(4-dimethylaminostyryl)-4*H*-pyran), which was pumped by a XeCl excimer laser at 308 nm. The photolysis and probe laser beams propagated antiparallel through the cells, and the fluorescence light, after passing through a band-pass filter ($\lambda = 330 \pm 10$ nm full width at half-maximum), was detected perpendicular to the beam axis with a photomultiplier tube. The photomultiplier signal was amplified, integrated in a boxcar integrator, digitized, and further processed on a personal computer. The delay between the photolysis and fluorescence excitation laser pulse was controlled with a delay generator. Depending on the quality of the LIF signal, the results from 2−10 experiments were averaged for a given time delay. The repetition rate was varied between 2 and 10 Hz. We set the gas flow high enough to allow for a complete exchange of the gas mixture in the reaction cell between two subsequent laser pulses.

2.2. Experiments at Pressures below 1 bar. For the experiments between 10 and 800 mbar at temperatures from 251 to 293 K, a cylindrical cell (low-pressure cell) made of stainless steel was used with a length of 23 cm and an inner volume of ∼640 cm^3. The cell is enclosed in a cooling jacket, which can be flushed with cold nitrogen. Before the test gas mixture enters the reaction cell, it passes a precooling arrangement consisting of a helically arranged copper capillary also enclosed in a cooling jacket. The entire setup is embedded in a housing, which can be evacuated to avoid condensation of water on the windows and to improve thermal insulation of the cooled parts. The temperature of the gas mixture was measured with two NiCr−Ni thermocouples in the gas flow at the entrance and exit of the reaction cell. The temperature difference between these two points never exceeded 2 K. The pressure of the gas mixture was measured with a capacitance manometer and regulated by active feedback control with a butterfly valve positioned after the cell. The reaction mixture was prepared in situ before the entrance of the cell by merging three separate gas flows (NCN_3 in He, NO in He, and additional He as bath gas) regulated by calibrated mass flow controllers.

2.3. Experiments at Pressures above 1 bar. The reaction cell (high-pressure cell) for our experiments between 1 and 50 bar at temperatures from 293 to 487 K has been already described elsewhere[32−34] and is only briefly characterized here. The reactor can be heated with a resistance heater, and the temperature of the reaction mixture is measured with two NiCr−Ni thermocouples at the entrance and the exit of the reaction zone. The temperature difference between these two points never exceeded 3 K. The pressure was measured with a pressure transducer, and the flow rate was controlled with a high-pressure mass flow controller positioned after the cell. For these high-pressure experiments, appropriate mixtures of NCN_3/NO/He were prepared in gas cylinders and allowed to homogenize for at least 12 h before use. The values obtained for k_3 did not show any systematic dependence on the filling level of the gas cylinders, which confirms the homogeneity of the gas mixtures.

2.4. Synthesis and Purity of the Substances. NCN_3 was synthesized by the reaction of NaN_3 with BrCN.[27,35] Because NCN_3 is highly explosive as a solid or liquid,[35] we chose a synthesis procedure,[27] which allows us to directly collect NCN_3 as a gas.

Finely powdered NaN_3 was filled in a 15 cm Vigreux column, fixed with glass wool, and degassed for at least 2 h under vacuum. Afterward, a 50 mL glass flask containing 0.8 g of BrCN was connected to the lower end of the column, evacuated, and the BrCN was allowed to react under its own vapor pressure with the NaN_3 in the column for at least 12 h. During this time, the BrCN completely disappeared, and the NaN_3 powder turned yellow from NCN_3 formation at the surface. The upper end of the Vigreux column was subsequently connected to an evacuated 2 L glass flask, in which the gaseous NCN_3 was collected.

Analysis of the reaction product with IR spectroscopy and mass spectrometry revealed minor contamination with BrCN. However, as is discussed below, this does not influence our results, and in view of the problematic handling of NCN_3 in the condensed phase, we did not attempt further purification. The purities of the other gases were as follows: He > 99.999%, NO > 99.5%.

3. RESULTS AND DISCUSSION

3.1. Experimental Results. In the low-pressure cell, experiments were performed at pressures ranging from 10 to 800 mbar and temperatures between 251 and 293 K. In the high-pressure cell, the pressure was varied between 2 and 49 bar at temperatures from 293 to 487 K. We were not able to detect NCN below 250 K potentially due to a too low vapor pressure of NCN_3. Above ~490 K the LIF signal of NCN showed an increasingly worse signal-to-noise ratio, presumably because thermal decomposition of NCN_3 starts to be no longer negligible at these conditions.[18] For the specific conditions of each experiment see Table 1S of the Supporting Information.

Typical fluorescence intensity−time profiles are displayed in Figures 2 and 3. From the linearized plots it is obvious that

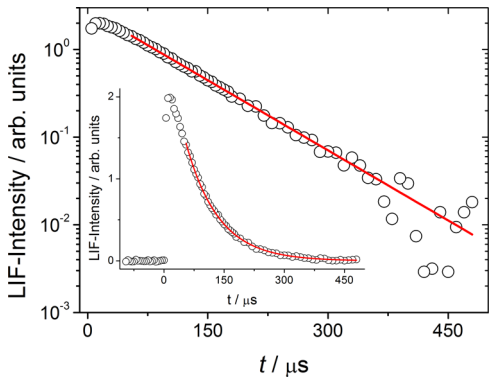

Figure 2. Fluorescence intensity−time profile and least-squares fit at T = 281 K, P = 100 mbar, and $[NO]_0 = 6.8 \times 10^{15}$ cm^{-3}.

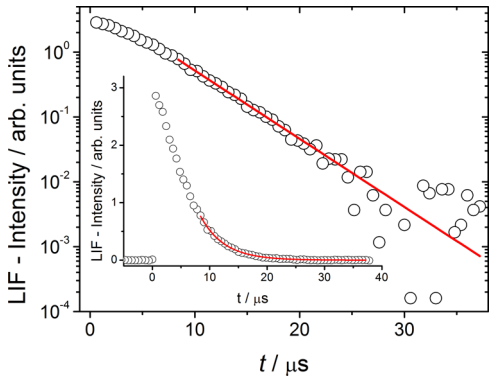

Figure 3. Fluorescence intensity−time profile and least-squares fit at T = 362 K, P = 12.2 bar, and $[NO]_0 = 3.2 \times 10^{16}$ cm^{-3}.

initial periods occur, in which the NCN decay is not monoexponential. This behavior was observed for photolysis at both 193 and 248 nm. A possible reason might be that NCN_3 photolysis forms electronically excited $NCN(^1\Delta_g)$,[28] which has to be collisionally quenched to the ground $^3\Sigma_g^-$ state before detection with our LIF setup. Interestingly, such induction periods were not mentioned in the work of Huang et al.[21] even though the same NCN precursor and the same LIF detection scheme was used. From absorption measurements of ^{1}NCN and ^{3}NCN after NCN_3 photolysis, Dammeier and Friedrichs[18] estimated an electronic quenching rate coefficient of ~1 × 10^{-15} cm^3 s^{-1} for T = 298 K with Ar as the collider gas. Assuming a similar value for He as collider, electronic relaxation times on the order of several hundred microseconds would be expected in our low-pressure experiments, which we did clearly not observe. The reason for the apparently much faster quenching in our experiments is probably the much more efficient quenching by NO as compared to He[21] or Ar,[18] because $NCN(^1\Delta_g) + NO(^2\Pi) \rightarrow NCN(^3\Sigma_g^-) + NO(^2\Pi)$ is a spin-allowed process. In their very recent work, Dammeier and Friedrichs[25] obtained pseudo-first-order rate coefficients in the range of 10^5−10^6 s^{-1} for the quenching of $NCN(^1\Delta_g)$ in Ar/NO mixtures with NO concentrations similar to those in our experiments but at higher temperatures (between 667 and 1500 K). In our experiments we found that the initial rise in the ^{3}NCN fluorescence−time profile became substantially faster with increasing NO concentration, but a quantitative analysis gave inconsistent results. In contrast to the shock tube experiments, where the precursor NCN_3 is decomposed completely and instantaneously on the experimental time scale, only a small fraction of NCN_3 is photolyzed in our experiments. The remaining NCN_3 may also act as a quencher with a completely unknown efficiency.

In view of these uncertainties and lacking data, we chose an operational approach and determined pseudo-first-order rate coefficients k_3' only at later reaction times, neglecting the nonlinearity of the semilogarithmic plots at the initial stages of the decays (cf. Figures 2 and 3). The values for k_3' were obtained from the slopes of linear fits $\log(I)$ vs t where I is the fluorescence intensity:

$$k_3' = \frac{\mathrm{d}\log(I)}{2.303\ \mathrm{d}t} \tag{1}$$

and the second-order rate coefficient k_3 was obtained from the relation

$$k_3 = \frac{k'_3}{[NO]} \tag{2}$$

Possible interferences from NCN loss processes other than reaction R3 were assessed by photolyzing gas mixtures of NCN_3 in He in the absence of NO. Except at the lowest pressures (where diffusion of NCN out of the detection volume might become relevant), the decay of NCN was much slower than the decay observed in the presence of NO. This result is a strong indication that reactions of NCN with BrCN (residual from NCN_3 synthesis) and NCN_3, as well as radical−radical reactions and diffusion of NCN out of the detection volume are unimportant under our conditions. We also varied the initial concentration of NCN_3 and found no influence on the NCN decays. The dependence of the values obtained for k_3 on the NO concentration is exemplarily displayed in Figure 4. The good linearity and the vanishing intercept of the fit provide further evidence that competing processes do not significantly influence our results.

The resulting rate coefficients k_3 determined from eq 2 are listed along with the detailed experimental conditions in Table 1S of the Supporting Information. Averaged values are plotted in Figure 5 as a function of pressure for various temperatures. We estimated a combined error of ±30% in the experimental values of k_3 from the fits and from the uncertainty in the initial NO concentration, which is illustrated by representative error bars in Figure 5. We note that, for the sake of clarity, our own experimental values were lumped together as indicated in the figure caption. Furthermore, the results for T < 260 K, 265 K < T < 277 K, and 283 K < T < 292 K were omitted in Figure 5. Available experimental data from the literature are also displayed, and our results for pressures below 1 bar agree

dx.doi.org/10.1021/jp303069g | J. Phys. Chem. A 2012, 116, 7293−7301

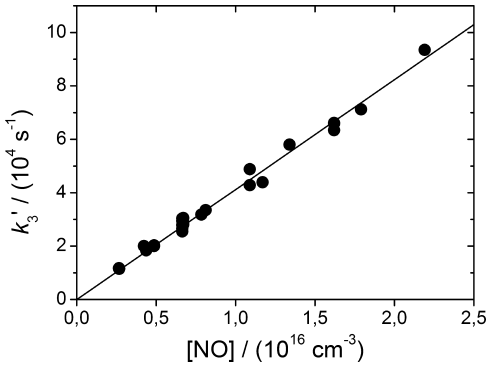

Figure 4. Dependence of the pseudo-first-order rate coefficient k_3' on the NO concentration (T = 293 K and P = 500 mbar). From the slope of the linear fit, a value of k_3 = (4.12 ± 0.04) × 10^{-12} cm^3 s^{-1} is obtained.

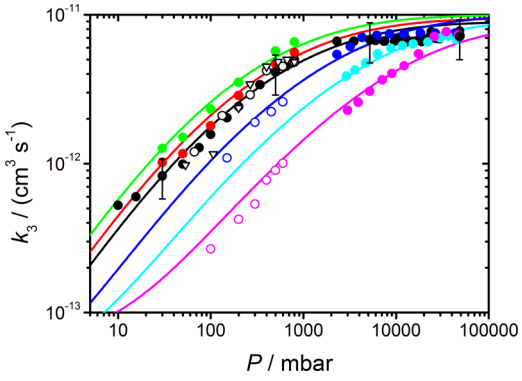

Figure 5. Temperature and pressure dependence of the rate coefficient k_3: (filled circles) experimental results from this work; (solid lines) master equation modeling from this work; (green) T = 263 ± 3 K; (red) T = 280 ± 3 K; (black) T = 293 ± 1 K; (blue) T = 362 ± 1 K; (cyan) T = 420 +7/−5 K; (magenta) T = 485 +2/−5 K; (black open circles) ref 19, T = 298 K; (blue open circles) ref 19, T = 373 K; (magenta open circles) ref 19, T = 473 K; (black open triangles) ref 21, T = 298 K.

well with these literature data. Furthermore, a reasonable consistency of the pressure dependence of our rate coefficients determined at pressures above 1 bar with the rate coefficients from low-pressure experiments of refs 19 and 21 for similar temperatures is obvious.

3.2. Master Equation Modeling. The observed temperature and pressure dependence of k_3 displayed in Figure 5 indicates a mechanism involving formation of an adduct[36] as was already suggested by Baren and Hershberger[19] and later confirmed by other authors.[21,23,24] At the highest pressures of our study, we obtained rate coefficients of k_3 ∼ 8 × 10^{-12} cm^3 s^{-1} virtually independent of temperature and pressure, which can be taken as an indication for a barrierless association step via a loose transition state with a rate coefficient at or near its high-pressure limit. At lower pressures, we observe falloff effects and a negative temperature dependence of k_3.

To relate our experimental results to the proposed mechanism from refs 21, 23, and 24, we modeled our results with a master equation on the basis of the potential energy diagram displayed in Figure 1.[21] The resulting detailed reaction mechanism consists of eqs R6−R11. We assumed in accordance with ref 21 that the internal conversion processes (R8) and (R9) are fast, i.e., not rate-determining. Furthermore, we did not distinguish between *trans*-NCNNO(^{2}A′) and *cis*-NCNNO(^{2}A′) but treated these conformers as one species with a hindered internal rotation about the N−N bond. This approach is justified and in fact even more adequate than a separate treatment of the individual isomers within the harmonic oscillator approximation, because the rotational barrier is well below the energy of the entrance and exit channels, and accordingly the cis−trans isomerization is much faster than the other unimolecular steps. As a consequence, only the lowest exit channel from NCNNO(^{2}A′) to CN + N_2O with a threshold energy of 143.9 kJ mol^{-1} relative to the trans isomer[21] needs to be considered. In summary, this means that the reaction mechanism within our model is approximated by the reversible association/dissociation step R4/R-4 via a loose transition state and by the consecutive elimination step (R5) via a tight transition state.

The modeling was performed in complete analogy to our approach described in ref 37. We expressed $k_3(T,P)$ as a product of the high-pressure limiting rate coefficient $k_3^\infty(T)$ ∼ $k_4^\infty(T)$ and a pressure- and temperature-dependent yield factor $Y(T,P)$:[36,37]

$$k_3(T,P) = k_4^\infty(T)\, Y(T,P) = k_4^\infty(T)\frac{D_5(T,P) + S(T,P)}{D_{-4}(T,P) + D_5(T,P) + S(T,P)} \quad (3)$$

where $S(T,P)$ is the rate of collisional stabilization of the intermediate NCNNO, and $D_i(T, P)$ is the rate of reaction of the unimolecular step i (i = −4, 5):

$$D_i(T,P) = \int_0^\infty k_i(E)\, n(E;T,P)\, dE \quad (4)$$

Here $n(E; T, P)$ is the steady-state population of NCNNO and $k_i(E)$ are the specific rate coefficients, which were obtained from the simplified statistical adiabatic channel model (SACM)[38] for reaction R-4 (loose transition state) and from RRKM theory[39−41] for reaction R5 (tight transition state). The molecular and transition state data required are collected in

Table 1. Molecular Parameters Used in the Master Equation Modeling (ω_i, Harmonic Wavenumbers; B_i, Rotational Constants; q_{el}, Electronic Partition Functions; $E_{0,rel}$, Energies at 0 K Relative to ^{3}NCN + NO), from Ref 21 Unless Noted Otherwise

species	ω_i (cm^{-1})	B_i (cm^{-1})	q_{el}	$E_{0,rel}$ (cm^{-1})
NCN	440, 440, 1272, 1563	0.40	3	
NO	1980	1.71	2 + 2 exp(−174 K/T)[a]	
trans-NCNNO (^{2}A′)	203, 242,[b] 521, 545, 637, 1028, 1345, 1681, 2319	2.69, 0.093, 0.089	2	−10860
TS(R5) ≡ TS(R10)[c]	367i, 66, 87, 240, 516, 569, 1278, 2150, 2201	1.02, 0.082, 0.076	2	1170

[a]Reference 48. [b]Omitted, torsional mode treated as a hindered rotor (see text), potential energy: $V(\varphi) = \sum_{k=0}^{10} V_k \cos(k\varphi)$ with V_0 = 3782, V_1 = −1007.7, V_2 = −2713, V_3 = −148.25, V_4 = 79.20, V_5 = −3.689, V_6 = 9.048, V_7 = 11.776, V_8 = −8.308, V_9 = −4.254, and V_{10} = 2.877 (units: cm^{-1}). [c]TS: transition state

dx.doi.org/10.1021/jp303069g | J. Phys. Chem. A 2012, 116, 7293−7301

Table 1. We based our SACM analysis of reaction R4/R-4 on the ^{2}A′ electronic state of NCNNO and calculated the specific rate coefficients $k_{-4}(E)$ for thermally averaged angular momentum quantum numbers $\langle J\rangle$ of NCNNO, which ranged from $\langle J\rangle(T$=263K) = 44 to $\langle J\rangle(T$=485K) = 60. The interpolation parameter of SACM, α/β,[38] was fitted to our experimental results (see below). Note that α/β is the same for k_4 and k_{-4}, because these rate coefficients are related by detailed balancing. In the case of reaction R5, a value of $\langle J\rangle$(293K) = 47 was used for all temperatures, because the J dependence of $k_5(E)$ is small (tight transition state). Sums and densities of states were determined by direct counting procedures.[38,40−42]

In calculating the density of states of NCNNO, the torsional mode about the N−N bond was treated as a one-dimensional hindered internal rotation as was already mentioned above. For the calculation of the hindered rotor energy levels, we followed the procedure described in ref 34. The torsional potential was obtained form a one-dimensional scan of the potential energy surface at the level of density-functional theory (DFT)[43] with the B3LYP[44] functional and the split-valence 6-31G(d) basis set[45] and fitted to a Fourier series. The Fourier coefficients representing the torsional potential are given in Table 1 (footnote b). The hindered rotor energy levels were convoluted with the harmonic density of states by using the Stein−Rabinovitch algorithm.[46] The quantum chemical calculations were performed with the Gaussian 03 program suite.[47]

The population $n(E;T,P)$ of the intermediate NCNNO is obtained by solving the steady-state master equation[37,40,41]

$$R_4 f(E) - \omega n(E) + \omega \int_0^\infty P(E,\varepsilon) n(\varepsilon) \mathrm{d}\varepsilon - [k_{-4}(E) + k_5(E)] n(E) = 0 \quad (5)$$

for given values of T and P. Here $f(E)$ is the nascent distribution of NCNNO formed in reaction R4 with a rate R_4[40,41] and is calculated as the Boltzmann-averaged sum of states $W_4(E - E_{0(-4)})$ with W_4 from SACM (for details see ref 37). For the transition probabilities $P(E,\varepsilon)$, a stepladder model obeying detailed balancing was used,[40,41] and the Lennard-Jones collision frequency ω was calculated with the following parameters:[40,41] ε(He)/k_B = 10.22 K,[49] σ(He) = 2.55 Å,[49] ε(NCNNO)/k_B = 201 K,[21] and σ(NCNNO) = 4.04 Å.[21] The step size of the stepladder model, ΔE_{SL}, which corresponds to the average energy transferred per down collision, was treated as an adjustable parameter.

Equation 5 is set up in discrete form with a grain size of 10 cm^{-1} and solved by standard routines for tridiagonal matrices.[50] For the calculation of the yield factor $Y(T,P)$ in eq 3, only relative unimolecular rates D_i/R_4 are needed because R_4 cancels. Accordingly, eq 5 is formally divided by R_4 before solution.[37] The relative rate of collisional stabilization is then obtained from the steady-state condition $S/R_4 = 1 - D_{-4}/R_4 - D_5/R_4$. More details of our approach can be found in ref 37. The results of our master equation modeling for ΔE_{SL} = 500 cm^{-1} are shown in Figure 5.

3.3. Discussion. Figure 5 shows that the agreement between our experimental results and the experimental data from the literature[19,21] for T = 295 ± 3 K is satisfactory and within our estimated uncertainty of ±30%. It is also obvious that the results from our master equation modeling give an adequate representation of the experimentally determined rate coefficients over the complete temperature and pressure range. In the following we will elucidate the general approach of our master equation analysis and derive a compact parametrization of $k_3(T,P)$ for modeling purposes. In this context it is important to keep in mind that there are two adjustable parameters within our model: the interpolation parameter of SACM, α/β, and the step size of the stepladder model, ΔE_{SL}. We note that the influence of α/β is essentially restricted to the high-pressure limit $k_3^\infty \sim k_4^\infty$, whereas ΔE_{SL} governs the pressure-dependent part of $k_3(T,P)$.

We started our analysis with the observation that the experimental results for $k_3(T,P)$ exhibit virtually no temperature dependence at the highest pressures (cf. Figure 5), which reflects a very weak temperature dependence of the high-pressure limit k_3^∞. Together with the absolute values of k_3^∞ on the order of 10^{-11} cm^3 s^{-1}, such behavior is typical for a barrierless radical−radical recombination reaction.

By varying the two parameters, α/β and ΔE_{SL}, we first fitted $k_3(T$=293K,$P)$ calculated from eqs 3−5 with $k_4^\infty(T)$ from the canonical version of SACM[51] to the experimental data set for T = 295 ± 3 K. From these fits we obtained optimized parameters of α/β = 0.39 and ΔE_{SL} = 500 cm^{-1}. The result for α/β is within the usual range $0.3 < \alpha/\beta < 0.6$.[52] The value obtained for ΔE_{SL} has to be compared with average energies transferred per down collision for He as collider gas. Such values are available for a number of different excited molecules and exhibit a considerable scatter between 175 and 740 cm^{-1} [53] with still lower values for photochemically excited hydrocarbons and CS_2.[40,53−55] Because ΔE_{SL} is correlated to the specific rate coefficients $k_{-4}(E)$ and $k_5(E)$ via eq 5 in our model, and hence to the quality of the potential energy surface, a quantitative comparison of our results for ΔE_{SL} to literature values is problematic. Nevertheless, the obtained value ΔE_{SL} = 500 cm^{-1} is in a reasonable order of magnitude.

When we used α/β = 0.39 to calculate $k_3(T,P)$ for other temperatures, we obtained a somewhat too strong, positive temperature dependence of $k_3^\infty(T) \sim k_4^\infty(T)$, which is typical for the canonical version of the simplified SACM.[52] The major reason is the use of a Morse function for the radial part of the potential between the recombining species, which has a too weak long-range part. The use of more realistic potentials, however, in particular for a reactant pair like ^{3}NCN + ^{2}NO, with different electronic states involved, is far beyond the scope of the present work and is also not justified in view of other simplifications made. Therefore, in an ad hoc approach, we kept α/β = 0.39 fixed in the calculation of $k_{-4}(E)$ (see above) and fitted $k_4^\infty(T)$ to the experimental data obtained at high pressures. Nearly temperature-independent values $k_4^\infty(T) \sim (0.95 \pm 0.05) \times 10^{-11}$ cm^3 s^{-1} were obtained, which are compared in Table 2 to the results from canonical SACM with α/β = 0.39. Although the differences are small, the too strong

Table 2. High-Pressure Limit $k_4^\infty(T)$ from Canonical SACM (α/β = 0.39) and from Fits to the Experiments

	$k_4^\infty/(10^{-11}$ cm^3 s$^{-1})$	
T (K)	SACM	fitted
263	0.81	1.0
280	0.83	0.95
293	0.85	0.90
362	0.94	1.0
420	1.01	0.95
485	1.08	0.90

positive temperature dependence of the SACM results, which is not observed in our experiments, becomes obvious.

Huang et al.[21] performed unimolecular rate theory calculations, using different codes to analyze the experimental results of their own work and from ref 19. Falloff curves were calculated at T = 298 K for He and N_2 as bath gases, and a high-pressure limiting value of $k_3^\infty > 3 \times 10^{-11}$ cm^3 s^{-1} was obtained from their variational transition state theory/master equation calculations (see Figure 5 of ref 21). This value, which is more than a factor of 3 higher than our experimental result, obviously had to be compensated for by a correspondingly lower value of $\langle \Delta E \rangle_{down}$ = 110 cm^{-1} to reproduce the rate coefficients determined in the pressure range 40−800 mbar, where k_3 is pressure-dependent. This result nicely illustrates the correlation between k_3^∞ and $\langle \Delta E \rangle_{down}$ and demonstrates the necessity of high-pressure experiments for reliable parametrizations.

As a complex-forming bimolecular reaction, NCN + NO should generally exhibit an s-shaped falloff curve with a pressure-independent low-pressure limit, which arises from the forward reaction of the chemically activated intermediate complex.[36] Evidence for this behavior within our model can be found in Figure 5, where the calculated falloff curve for the highest temperature shows some deviation from linearity at low pressures. Measurements below 10 mbar and at elevated temperatures, outside the parameter range of the present study, would be necessary to experimentally confirm this effect.

The difference between the high- and low-pressure limiting rate coefficient and the location of the transition range between them as a function of temperature and pressure depend in a complex way on the difference of the threshold energies $E_{0(-4)} - E_{0(5)}$, on the looseness of the corresponding transition states, on the well depth of the intermediate, NCNNO, and on the collisional energy transfer, which is characterized in our model by ΔE_{SL}. The general relations are elucidated in ref 36, and detailed examples can be found in refs 37 and 56.

Keeping this complexity and the limited knowledge on key features of the potential energy surface in mind, we refrain from a more detailed theoretical analysis but cast the available experimental results into a parametrization proposed by Troe[57] for use in kinetic modeling. The analysis of Huang et al.[21] as well as our master equation calculations indicate that the NCN + NO reaction is dominated by recombination to form NCNNO at pressures above 30 mbar and temperatures below 485 K. Accordingly, the pressure dependence of the rate coefficient in this parameter range can be written as a modified Lindemann−Hinshelwood expression:[40,41,57]

$$k_3(T,P) = k_4^\infty \frac{k_4^0[\mathrm{M}]}{k_4^0[\mathrm{M}] + k_4^\infty} F \tag{6}$$

with

$$\log F = \frac{\log F_C}{1 + \left[\frac{\log(k_4^0[\mathrm{M}]/k_4^\infty)}{0.75 - 1.27 \log F_C}\right]^2} \tag{7}$$

Here, k_4^0 and k_4^∞ are the low- and high-pressure limiting rate coefficients of reaction R4, respectively, and F_C represents a broadening factor, which accounts for deviations from the falloff behavior predicted by the simple Lindemann−Hinshelwood model. The following parametrization adequately reproduces the experimental data over the entire parameter range as shown in Figure 6:

$$k_4^0[\mathrm{M{=}He}] = 1.91 \times 10^{-30} \left(\frac{T}{300\ \mathrm{K}}\right)^{-3.3} \mathrm{cm}^6\ \mathrm{s}^{-1}\ [\mathrm{He}] \tag{8}$$

$$k_4^\infty = 1.12 \times 10^{-11} \exp\left(-\frac{23\ \mathrm{K}}{T}\right) \mathrm{cm}^3\ \mathrm{s}^{-1} \tag{9}$$

$$F_C = 0.28 \exp\left(\frac{173\ \mathrm{K}}{T}\right) \tag{10}$$

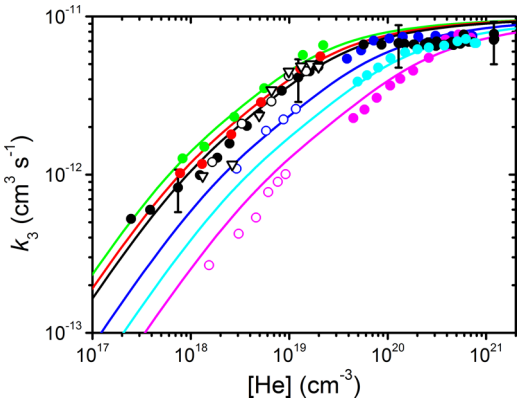

Figure 6. Comparison of the experimental results for k_3 to the parametrization according to eqs 6−10: (symbols) experimental data identical to those in Figure 5; (solid lines) empirical representation by eqs 6−10.

From a comparison with our master equation calculations, it follows that this parametrization is adequate at least for temperatures between 250 and 500 K and pressures between 30 mbar and 50 bar with an estimated uncertainty of 30%. We note that k_4^∞ from eq 8 is about 10% higher than the values from our master equation modeling with a slightly different temperature dependence.

In view of the simplifications in our model, an extrapolation of the rate coefficient k_3 to temperatures markedly above the upper limit of our experimental range is not appropriate. We note, however, that a comparison of our data with the results from Dammeier and Friedrichs[25] indicates a minimum of k_3 at temperatures between 500 and 750 K. Such a global behavior was already predicted from calculations in ref 21. Any more detailed description, however, would require much more detailed information on the underlying potential energy surface. In particular, the nonadiabatic transitions between the ^{2}A″ and ^{2}A′ electronic states of NCNNO and the multiwell character of the low-lying ^{2}A′ state would have to be taken into account (Figure 1). The experimental data from refs 19 and 21, and from the present work together with the high-temperature data from ref 25 can form the experimental basis for such a comprehensive analysis.

4. CONCLUSIONS

The kinetics of the NCN + NO reaction (R3) were studied over a broad temperature (251 K ≤ T ≤ 487 K) and pressure range (30 mbar ≤ P ≤ 50 bar). Rate coefficients close to the high-pressure limiting values could be experimentally determined for the first time. With a master equation analysis on the basis of a simple complex-forming mechanism and quantum chemical data of Huang et al.,[21] the experimentally observed temperature and pressure dependence of the rate coefficient k_3

could be adequately reproduced. A parametrization was performed, eqs 6−10, to cast $k_3(T,P)$ into a form useful for kinetic modeling.

■ ASSOCIATED CONTENT

Supporting Information

Conditions and rate coefficients for the individual experiments. This information is available free of charge via the Internet at http://pubs.acs.org.

■ AUTHOR INFORMATION

Corresponding Author

*E-mail: matthias.olzmann@kit.edu.

Present Address

[†]Combustion Research Facility, Mail Stop 9055, Sandia National Laboratories, Livermore, California 94551−0969.

Notes

The authors declare no competing financial interest.

■ ACKNOWLEDGMENTS

We thank Prof. F. Breher and Dr. I. Krummenacher for help with the NCN_3 synthesis. Support of this work from the Deutsche Forschungsgemeinschaft (SFB 606 "Non-stationary Combustion: Transport Phenomena, Chemical Reactions, Technical Systems") is gratefully acknowledged. O.W. received financial support by the "Concept for the Future" program at Karlsruhe Institute of Technology within the German Excellence Initiative.

■ REFERENCES

(1) Warnatz, J.; Maas, U.; Dibble, R. W. *Combustion*, 3rd ed.; Springer: Berlin, 2001.
(2) Finlayson-Pitts, B. J.; Pitts, J. N., Jr. *Chemistry of the Upper and Lower Atmosphere*; Academic Press: San Diego, 2000.
(3) Fenimore, C. P. *Proc. Combust. Inst.* **1971**, *13*, 373.
(4) Miller, J. A.; Bowman, C. T. *Prog. Energy Combust. Sci.* **1989**, *15*, 287.
(5) Dean, A. M.; Bozzelli, J. W. In *Gas-Phase Combustion Chemistry*; Gardiner, W. C., Jr., Ed.; Springer: New York, 2000; p 125.
(6) Cui, Q.; Morokuma, K.; Bowman, J. M.; Klippenstein, S. J. *J. Chem. Phys.* **1999**, *110*, 9469.
(7) Moskaleva, L. V.; Lin, M. C. *Proc. Combust. Inst.* **2000**, *28*, 2393.
(8) Vasudevan, V.; Hanson, R. K.; Bowman, C. T.; Golden, D. M.; Davidson, D. F. *J. Phys. Chem. A* **2007**, *111*, 11818.
(9) Harding, L. B.; Klippenstein, S. J.; Miller, J. A. *J. Phys. Chem. A* **2008**, *112*, 522.
(10) Smith, G. P. *Chem. Phys. Lett.* **2003**, *367*, 541.
(11) Sutton, J. A.; Williams, B. A.; Fleming, J. W. *Combust. Flame* **2008**, *153*, 465.
(12) El Bakali, A.; Pillier, L.; Desgroux, P.; Lefort, B.; Gasnot, L.; Pauwels, J. F.; da Costa, I. *Fuel* **2006**, *85*, 896.
(13) Zsély, I. Gy.; Zádor, J.; Turányi, T. *Int. J. Chem. Kinet.* **2008**, *40*, 754.
(14) Konnov, A. A. *Combust. Flame* **2009**, *156*, 2093.
(15) Lamoureux, N.; Desgroux, P.; El Bakali, A.; Pauwels, J. F. *Combust. Flame* **2010**, *157*, 1929.
(16) Sutton, J. A.; Williams, B. A.; Fleming, J. W. *Combust. Flame* **2012**, *159*, 562.
(17) Dagaut, P.; Glarborg, P.; Alzueta, M. U. *Prog. Energy Combust. Sci.* **2008**, *34*, 1.
(18) Dammeier, J.; Friedrichs, G. *J. Phys. Chem. A* **2010**, *114*, 12963.
(19) Baren, R. E.; Hershberger, J. F. *J. Phys. Chem. A* **2002**, *106*, 11093.
(20) Smith, G. P.; Copeland, R. A.; Crosley, D. R. *J. Chem. Phys.* **1989**, *91*, 1987.
(21) Huang, C.-L.; Tseng, S. Y.; Wang, T. Y.; Wang, N. S.; Xu, Z. F.; Lin, M. C. *J. Chem. Phys.* **2005**, *122*, 184321.
(22) Mebel, A. M.; Morokuma, K.; Lin, M. C. *J. Chem. Phys.* **1995**, *103*, 7414.
(23) Chen, H.-T.; Ho, J.-J. *J. Phys. Chem. A* **2005**, *109*, 2564.
(24) Wei, Z. G.; Li, Q. S.; Zhang, S. W.; Sun, Y. B.; Sun, C. C. *J. Mol. Struct. (THEOCHEM)* **2005**, *722*, 139.
(25) Dammeier, J.; Friedrichs, G. *J. Phys. Chem. A* **2011**, *115*, 14382.
(26) Wang, N. S.; Yang, D. L.; Lin, M. C.; Melius, C. F. *Int. J. Chem. Kinet* **1991**, *23*, 151.
(27) Milligan, D. E.; Jacox, M. E.; Bass, A. M. *J. Chem. Phys.* **1965**, *43*, 3149.
(28) Kroto, H. W. *J. Chem. Phys.* **1966**, *44*, 831.
(29) Okabe, H.; Mele, A. *J. Chem. Phys.* **1969**, *51*, 2100.
(30) Baumgärtel, S.; Gericke, K.-H.; Comes, F. J. *Ber. Bunsen-Ges. Phys. Chem.* **1994**, *98*, 1009.
(31) Smith, G. P.; Copeland, R. A.; Crosley, D. R. *J. Chem. Phys.* **1989**, *91*, 1987.
(32) Forster, R.; Frost, M.; Fulle, D.; Hamann, H. F.; Hippler, H.; Schlepegrell, A.; Troe, J. *J. Chem. Phys.* **1995**, *103*, 2949.
(33) Hippler, H.; Striebel, F.; Viskolcz, B. *Phys. Chem. Chem. Phys.* **2001**, *3*, 2450.
(34) Welz, O.; Striebel, F.; Olzmann, M. *Phys. Chem. Chem. Phys.* **2008**, *10*, 320.
(35) Marsh, F. D.; Hermes, M. E. *J. Am. Chem. Soc.* **1964**, *86*, 4506.
(36) Troe, J. *J. Chem. Soc., Faraday Trans.* **1994**, *90*, 2303.
(37) Delbos, E.; Fittschen, C.; Hippler, H.; Krasteva, N.; Olzmann, M.; Viskolcz, V. *J. Phys. Chem. A* **2006**, *110*, 3238.
(38) Troe, J. *J. Chem. Phys.* **1983**, *79*, 6017.
(39) Marcus, R. A.; Rice, O. K. *J. Phys. Colloid. Chem.* **1951**, *55*, 894.
(40) Gilbert, R. G.; Smith, S. C. *Theory of Unimolecular and Recombination Reactions*; Blackwell: Oxford, U.K., 1990.
(41) Holbrook, K. A.; Pilling, M. J.; Robertson, S. H. *Unimolecular Reactions*, 2nd ed.; Wiley: Chichester, U.K., 1996.
(42) Beyer, T.; Swinehart, D. F. *Commun. ACM* **1973**, *16*, 379.
(43) Parr, R. G.; Yang, W. *Density-functional theory of atoms and molecules*; Oxford University Press: Oxford, U.K., 1989.
(44) Becke, A. D. *J. Chem. Phys.* **1993**, *98*, 5648.
(45) Hehre, W. J.; Radom, L.; Pople, J. A.; Schleyer, P. v. R. *Ab Initio Molecular Orbital Theory*; Wiley: New York, 1987.
(46) Stein, S. E.; Rabinovitch, B. S. *J. Chem. Phys.* **1973**, *58*, 2438.
(47) Frisch, M. J.; Trucks, G. W.; Schlegel, H. B.; Scuseria, G. E.; Robb, M. A.; Cheeseman, J. R.; Montgomery, J. A., Jr.; Vreven, T.; Kudin, K. N.; Burant, J. C.; Millam, J. M.; Iyengar, S. S.; Tomasi, J.; Barone, V.; Mennucci, B.; Cossi, M.; Scalmani, G.; Rega, N.; Petersson, G. A.; Nakatsuji, H.; Hada, M.; Ehara, M.; Toyota, K.; Fukuda, R.; Hasegawa, J.; Ishida, M.; Nakajima, T.; Honda, Y.; Kitao, O.; Nakai, H.; Klene, M.; Li, X.; Knox, J. E.; Hratchian, H. P.; Cross, J. B.; Bakken, V.; Adamo, C.; Jaramillo, J.; Gomperts, R.; Stratmann, R. E.; Yazyev, O.; Austin, A. J.; Cammi, R.; Pomelli, C.; Ochterski, J. W.; Ayala, P. Y.; Morokuma, K.; Voth, G. A.; Salvador, P.; Dannenberg, J. J.; Zakrzewski, V. G.; Dapprich, S.; Daniels, A. D.; Strain, M. C.; Farkas, O.; Malick, D. K.; Rabuck, A. D.; Raghavachari, K.; Foresman, J. B.; Ortiz, J. V.; Cui, Q.; Baboul, A. G.; Clifford, S.; Cioslowski, J.; Stefanov, B. B.; Liu, G.; Liashenko, A.; Piskorz, P.; Komaromi, I.; Martin, R. L.; Fox, D. J.; Keith, T.; Al-Laham, M. A.; Peng, C. Y.; Nanayakkara, A.; Challacombe, M.; Gill, P. M. W.; Johnson, B.; Chen, W.; Wong, M. W.; Gonzalez, C.; Pople, J. A. *Gaussian 03*; Revision C.02; Gaussian, Inc.: Wallingford, CT, 2004.
(48) Chase, M. W., Jr.; Davies C. A.; Downey, J. R., Jr.; Frurip, D. J.; McDonald, R. A.; Syverud, A. N. *J. Phys. Chem. Ref. Data* **1985**, *14*, Supplement No. 1.
(49) Reid, R. C.; Prausnitz, J. M.; Poling, B. E. *The Properties of Gases and Liquids*, 4th ed.; McGraw-Hill: Boston, U.S.A., 1987.
(50) Press, W. H.; Flannery, B. P.; Teukolski, S. A.; Vetterling, W. T. *Numerical Recipes in Fortran*, 2nd ed.; Cambridge University Press: Cambridge, U.K., 1992.
(51) Troe, J. *J. Chem. Phys.* **1981**, *75*, 226.
(52) Cobos, C. J.; Troe, J. *J. Chem. Phys.* **1985**, *83*, 1010.

(53) Oref, I.; Tardy, D. C. *Chem. Rev.* **1990**, *90*, 1407.
(54) Dove, J. E.; Hippler, H.; Troe, J. *J. Chem. Phys.* **1985**, *82*, 1907.
(55) Rossi, M. J.; Pladziewicz, J. R.; Barker, J. R. *J. Chem. Phys.* **1983**, *78*, 6695.
(56) Fulle, D.; Hamann, H. F.; Hippler, H.; Troe, J. *J. Chem. Phys.* **1996**, *105*, 983.
(57) Troe, J. *J. Phys. Chem.* **1979**, *83*, 114.